Petrick, C., Dobslaw, H., Bergmann, I., Schön, N., Matthes, K., Thomas, M. (2014): Low-frequency ocean bottom pressure variations in the North Pacific in response to time-variable surface winds. - *Journal of Geophysical Research*, *119*, 8, p. 5190-5202.

DOI: http://doi.org/10.1002/2013JC009635

AGU PUBLICATIONS

JGR

Journal of Geophysical Research: Oceans

RESEARCH ARTICLE

10.1002/2013JC009635

Low-frequency ocean bottom pressure variations in the North Pacific in response to time-variable surface winds

C. Petrick[1,2], H. Dobslaw[1], I. Bergmann-Wolf[1], N. Schön[1,3], K. Matthes[2], and M. Thomas[1,4]

[1]Deutsches GeoForschungsZentrum, Potsdam, Germany, [2]GEOMAR Helmholtz Centre for Ocean Research, Kiel, Germany, [3]Now at Bristol Glaciology Centre, School of Geographical Sciences, University of Bristol, Bristol, UK, [4]Institut für Meteorologie, Freie Universität Berlin, Berlin, Germany

Key Points:
- Low frequency ocean bottom pressure variability is observed by GRACE
- OBP in the North Pacific gyres is governed by the surface wind field
- Surface wind variability is characterized both by NAM and ENSO modes

Correspondence to:
H. Dobslaw,
dobslaw@gfz-potsdam.de

Citation:
Petrick, C., H. Dobslaw, I. Bergmann-Wolf, N. Schön, K. Matthes, and M. Thomas (2014), Low-frequency ocean bottom pressure variations in the North Pacific in response to time-variable surface winds, *J. Geophys. Res. Oceans*, *119*, 5190–5202, doi:10.1002/2013JC009635.

Received 20 NOV 2013
Accepted 21 JUL 2014
Accepted article online 24 JUL 2014
Published online 15 AUG 2014

Abstract One decade of time-variable gravity field observations from the GRACE satellite mission reveals low-frequency ocean bottom pressure (OBP) variability of up to 2.5 hPa centered at the northern flank of the subtropical gyre in the North Pacific. From a 145 year-long simulation with a coupled chemistry climate model, OBP variability is found to be related to the prevailing atmospheric sea-level pressure and surface wind conditions in the larger North Pacific area. The dominating atmospheric pressure patterns obtained from the climate model run allow in combination with ERA-Interim sea-level pressure and surface winds a reconstruction of the OBP variability in the North Pacific from atmospheric model data only, which correlates favorably (r=0.7) with GRACE ocean bottom pressure observations. The regression results indicate that GRACE-based OBP observations are indeed sensitive to changes in the prevailing sea-level pressure and thus surface wind conditions in the North Pacific, thereby opening opportunities to constrain atmospheric models from satellite gravity observations over the oceans.

1. Introduction

Observations of temporal variations of the Earth's gravity field from the satellite mission GRACE [*Tapley et al.* 2004] present a new way of monitoring a wide range of Earth system dynamics that are related to large-scale mass transports. Over the continents, the mission is in particular sensitive to several aspects of the terrestrial branch of the global water cycle: it allows to monitor the mass balance of continental ice-sheets and glaciers [*Jacob et al.* 2012], the deep soil moisture variability and its consequences for drought and flood potentials [*Houborg et al.* 2012], as well as groundwater depletion arising from growing water demands for irrigation and human consumption in various densely populated regions of our planet [*Voss et al.* 2013]. With GRACE still in operation and the GRACE Follow-On mission in preparation for launch in 2017, the observing concept is now in a good position to be considered as a contribution to the monitoring of "Essential Climate Variables" [*Hollmann et al.* 2013] as defined by the World Meteorological Organization.

Over the oceans, GRACE observations provide estimates of ocean bottom pressure (OBP) that allow to quantify the eustatic contribution to global sea-level rise [*Chambers and Willis* 2010]. In addition, regionally varying signals in response to predominant atmospheric conditions are found in several areas outside the tropics. In the Northern Pacific, for example, strong signals were found in the GRACE data all along the flank between the subpolar and the subtropical gyre. Those OBP changes have been discussed in terms of seasonal variations [*Bingham and Hughes* 2006], and also on interannual timescales [*Song and Zlotnicki* 2008]. Those previous studies conclude that the variability here is well explained by assuming that anomalies—i.e., deviations from the long-term mean—in barotropic ocean transports are in local balance with anomalies in the curl of the surface wind stress.

By means of a correlation analysis, the latter has been related to time variations of the tropical atmosphere-ocean phenomenon El Nino Southern Oscillation [*Chambers* 2011], without, however, identifying the actual physical mechanism [see, e.g., *Liu and Alexander* 2007] behind the suggested teleconnection. The secular trends as seen from GRACE in the same area have been, however, related to the Pacific Decadal Oscillation, which is a prominent mode of extratropical natural climate variability [*Cheng et al.* 2013]. Since regional sea-level in the North Pacific has risen over the period 1993–2010 with 5 mm/yr at a rate of about 1.5 times the global average [*Moon and Song* 2013], and OBP variability contributes a significant fraction to it, it is

important to clarify the dynamical mechanisms behind those changes in order to facilitate reliable sea-level predictions for the future.

Recently, substantial advancements in GRACE data accuracy [*Sakumura et al*. 2014] have been realized as the combined effect of various improvements in both the data processing of a number of different instruments aboard the spacecraft, as well as in the accuracy of several geophysical background models. Those improvements finally led to substantially more reliable OBP estimates from the GRACE release 05 gravity fields in particular on regional scales [*Chambers and Bonin* 2012]. This increase in accuracy and the now available full decade of data motivate us to revisit the question of what can be learned from OBP as observed by GRACE in the North Pacific about the low frequency atmosphere-ocean variability. For this, we utilize atmospheric reanalysis data from ERA-Interim [*Dee et al*. 2011], accompanied with simulated OBP from a general ocean circulation model driven by atmospheric conditions obtained from the same data set. The connections of OBP variability in the North Pacific to low-frequency climate phenomena are further evaluated by means of long-term simulations of the natural climate variability with a state-of-the-art coupled chemistry climate model, thereby allowing to discuss the information content GRACE might provide on the dynamical state of the climate system in the North Pacific area.

This work is structured as follows: section 2 describes all processing steps that are required to derive globally gridded ocean bottom pressure estimates from the time-variable gravity fields provided by the GRACE processing centers. Section 3 introduces the two numerical experiments we use to reconstruct OBP in the North Pacific: (i) from atmosphere and ocean state variables simulated with the climate model (section 4), and (ii) from reanalysis sea-level pressure fields. The OBP of the latter reconstruction is then directly compared to the GRACE observations (section 5). The relation of the observed low-frequency OBP variability is subsequently discussed with respect to a number of modes of natural climate variability (section 6) that are known to have an effect on the atmospheric conditions in the North Pacific area, before a summary is given in the final section.

2. GRACE Ocean Bottom Pressure Observations

We use release 05 of GRACE monthly gravity field models from Deutsches GeoForschungsZentrum (GFZ) in Potsdam, Germany [*Dahle et al*. 2012], which are publicly available at isdc.gfz-potsdam.de. The data are provided in terms of spherical harmonics that are complete to degree and order 90, and covers the time period from January 2003 to December 2012. The post processing necessary to transform the time variations of the gravity potential into gridded ocean bottom pressure estimates essentially follows the strategy chosen by *Bergmann and Dobslaw* [2012], which is briefly summarized here: First, we add mean annual harmonics of the degree-1 terms of the spherical harmonic expansion of the time-variable gravity field as obtained from satellite laser ranging observations [*Eanes* 2000], since GRACE gravity fields are realized in the center-of-mass reference frame and therefore do not provide variations of the geocenter. Further, we restore the monthly mean of the Atmosphere Ocean De-Aliasing Level-1B Product [AOD1B] [*Flechtner and Dobslaw* 2013] applied during the GRACE gravity field processing to account for high-frequency nontidal mass variability by readding the so-called GAC product, which is provided together with the monthly gravity field models.

Since only time variations of the gravity field are interpretable in terms of mass transport and thus OBP, we subtract from each monthly solution a long-term average over the 10 year period considered. Spatial leakage of continental mass variations is reduced by subtracting 300 km Gaussian averaged fields over all continental landmasses [*Wahr et al*. 1998]. In order to account for the systematic errors inherent in the GRACE observation geometry, an anisotropic two-point-kernel filter [DDK1; *Kusche* 2007] is applied, that also implicitly smoothes the signal in space to reduce noise. By assuming that the mass variability we are interested in is concentrated in a thin layer of mass at the surface of the Earth, anomalies in the gravity potential are unambiguously synthesized into gridded mass anomalies [*Wahr et al*. 1998], that are subsequently transformed into OBP anomalies by incorporating the hydrostatic equation.

In total, five monthly gravity fields are missing (June 2003, January 2011, June 2011, May 2012, and October 2012) from the GRACE time series. During those months, instrumental data quality is limited due to either environmental effects, low energy availability, or temporarily adverse orbit conditions that are typically related to transitional repeat orbits with revisiting times of a few days only, thereby implying a substantially

reduced spatial resolution of the global solutions. Next, we remove annual harmonics and secular trends for every location in the gridded data set. Changes in the total mass of the water stored in the ocean basins cause—apart from secondary effects, as self-attraction and loading [*Tamisiea et al*. 2010]—a globally homogeneous response in sea level and therefore also in OBP, as evidenced from numerical modeling studies [*Dobslaw and Thomas* 2007b; *Lorbacher et al*. 2012], and satellite [*Chambers and Willis* 2010] and in situ [*Hughes et al*. 2012] observations. Since we focus on regional OBP variability in this study, the global mean OBP of each month is removed from every GRACE OBP grid point.

OBP variability from GRACE that is detrended, deseasonalized, and reduced for the effects of global eustatic sea-level variations exhibits a standard deviation of up to 2.5 hPa along the northern flank of the subtropical gyre around 180° E and 42° N in the North Pacific (Figure 1a). Spatial cross-correlations of the OBP field with the time series at the point of the highest standard deviation (Figure 1b) indicate that the response is largely in phase throughout the whole area.

3. Numerical Experiments with CESM and OMCT

In order to investigate the relations between OBP and large-scale atmospheric variability in more detail, we utilize two different numerical model set-ups: a fully coupled chemistry climate model, and an ocean model forced with atmospheric boundary conditions from a global reanalysis.

The first experiment is performed with NCAR's Community Earth System Model [CESM, version 1.0.2; *Gent et al*. 2011], that includes interactively coupled components for the atmosphere [*Neale et al*. 2013], the ocean with sea ice [*Danabasoglu et al*. 2012], and the continental hydrosphere [*Lawrence et al*. 2011]. We use the atmospheric module WACCM within CESM, which includes 66 levels up to an altitude of 140 km [*Marsh et al*. 2013]. The horizontal resolution is 1.9° × 2.5° for the atmosphere, and approximately 1° for the curvilinear grid of the ocean module. In our experiment, we simulate the natural climate variability over 145 years by forcing it with a Solar Cycle that is spectrally resolved from the far-ultraviolet to the near-infrared which is projected into the future by repeating the cycles 20–23 from the years 1965 to 2008. The externally prescribed Quasi Biennial Oscillation is developed into Fourier coefficients based on observations from the years 1954 to 2004, and then projected into the future. Greenhouse gas concentrations and ozone depleting substances are kept constant on a 1960s level, and changes in atmospheric aerosol content due to major volcanic eruptions are not included. Atmospheric surface wind and pressure fields have been stored as monthly means for the whole timespan of the experiment. OBP is calculated from the vertical integral of the oceanic density and sea-level field following *Ponte* [1999]. Further details about this particular CESM experiment are given in *Petrick* [2013].

Although the CESM experiment is assumed to represent the typical atmosphere-ocean variability in a statistical sense, it cannot be expected to be directly comparable to observations in the time domain. We therefore employ a second experiment with the Ocean Model for Circulation and Tides [*Thomas et al*. 2001], that is forced with atmospheric fields obtained from ECMWF's most recent reanalysis ERA-Interim [*Dee et al*. 2011] for the period 1989–2012. OMCT is a direct descendant of the Hamburg Ocean Primitive Equation Model [*Drijfhout et al*. 1996; *Wolff et al*. 1997] that has been adjusted to the weather timescale and coupled with an ephemeral tidal module. The model is based on the non-linear balance equations for momentum, the continuity equation, and conservation equations for heat and salt. The hydrostatic and the Boussinesq approximations are applied. Sea-level, horizontal velocities, potential temperature, and salinity are calculated prognostically and vertical velocities are determined diagnostically from the incompressibility condition. The OMCT configuration applied in this study has a time step of 30 min, it is discretized on a 1.875° regular grid, with 13 layers in the vertical. OBP variability simulated by this OMCT set-up has been discussed in *Dobslaw and Thomas* [2007a], information on the decadal mean circulation is provided by *Dobslaw* [2007]. Note that lunisolar gravitational tides are not included in the OMCT experiment employed here.

As for the GRACE data, simulated OBP time-series from both model runs are detrended, deseasonalized, and reduced for effects due to variations in global eustatic sea level. Variability simulated by CESM in the North Pacific (Figure 1c) is spatially consistent with GRACE, highest standard deviations of 2.5 hPa are found at similar locations. OMCT mass anomalies have also comparable variabilities in the area (Figure 1e), although a second prominent peak is identified further west at 160° E. Nevertheless, spatial cross correlations with the time series at 180° E, 42° N are equally strong as for the GRACE data. Note that in the model

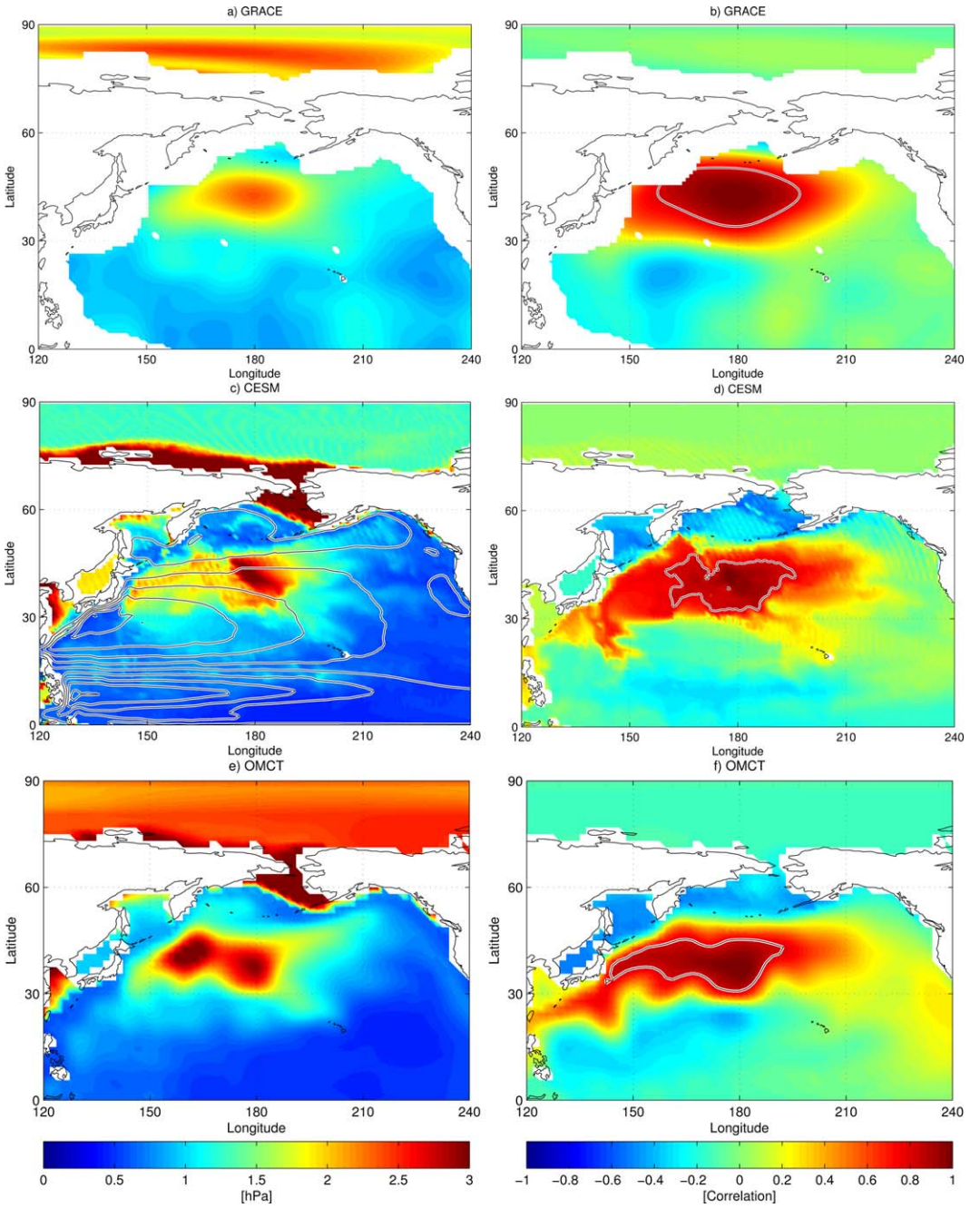

Figure 1. Standard deviation of the deseasonalized and detrended OBP variations in the North Pacific as observed from GRACE (a), and as simulated from CESM (c), and OMCT (e) numerical models; as well as spatial cross correlations of the OBP field from GRACE (b), CESM (d), and OMCT (e) with the corresponding OBP at location 180° E, 42° N. The chosen position represents the point with the highest standard deviation in the GRACE OBP field. White isolines indicate areas with standard deviations exceeding 1 hPa and spatial cross correlations larger than 0.7, where OBP has been averaged to obtain corresponding time series that are representing the low-frequency OBP variability in the area for GRACE observations and the two numerical experiments. In Figure 1c, isolines visualize the multiyear mean barotropic stream function in order to indicate the extend of the gyres as simulated in the CESM experiment.

results, boundaries between subtropical and subpolar gyres are more sharply defined than in the observations, which is related to the limited spatial resolution of GRACE after post processing with the DDK1 filter.

Since spatial cross correlations of low-frequency OBP from GRACE (Figure 1b) and both numerical experiments (Figures 1d and 1f) consistently indicate a spatially homogeneous OBP variability in the North Pacific, it is reasonable to describe this mass variability in the whole area by a scalar time-series only. For this, we select all locations with cross correlations with the central point of at least 0.7 and a standard deviation of

at least 1 hPa, and average the OBP over that region. In the following sections, we primarily focus on the time variability of the area-averaged OBP, and disregard any potential spatial variability within the area.

4. Reconstruction of OBP From CESM SLP

A theory for the seasonal variability of upper ocean dynamics that is still accepted has been synthesized by *Gill and Niiler* [1973]. By assuming Ekman dynamics near the surface, and geostrophy as well as Sverdrup dynamics in the interior, they found that gradients in the time-variable OBP are balanced by the sum of baroclinic processes associated with density changes in the water column and the ocean's response to time-varying surface winds [cf. *Gill and Niiler* 1973, equation 5.3]. By means of scaling arguments, the authors concluded that, outside the tropics, the barotropic response of the ocean to Ekman pumping is expected to lead to notable OBP variability, whereas closer to the equator baroclinic processes start to dominate, thereby largely compensating any wind effects on the OBP field.

Based on those theoretical arguments, we expect a strong influence of the surface winds on OBP anomalies. In the monthly mean average, winds in the free troposphere are almost always in geostrophic balance. Surface winds instead tend to cross isobars toward a low-pressure system, but they will nevertheless very close to the geostrophic winds in both magnitude and direction, thereby allowing us to use atmospheric sea-level pressure (SLP) as a scalar proxy for the surface winds. To identify the dominant pattern in SLP and thus surface wind, we compute the Empirical Orthogonal Functions (EOF) of the SLP anomalies in the northern hemisphere between 120° E and 240° E [*Petrick* 2013, equation (2.38)]. The associated Principal Components (PC) are each normalized by their standard deviation, leaving the EOF patterns directly comparable in amplitude. To additionally visualize the associated wind fields, each PC is regressed onto the zonal and meridional component of the surface wind velocities [*Petrick* 2013, equation (2.41)] and the corresponding patterns are overlaid to the four leading EOFs by means of arrows (Figure 2).

The first EOF of SLP is characterized by a high-amplitude region in the central North Pacific that is accompanied by an equally strong but anticorrelated signal over the Arctic. It is closely associated with the strength of the Aleutian Low and the Pacific North America Pattern [*Barnston and Livezey* 1987], and explains 36% of the total signal in the region considered. The second EOF—approximately in quadrature with the first—is related to the North Pacific Oscillation, and still accounts for about 20% of the overall signal variability. The third EOF is mainly located over land, with high amplitudes over Siberia and anticorrelated signals over Alaska at about the same magnitude. The last EOF considered here still explains about 8% of the total signal and contains covarying signals centered at the location of the Aleutian Low and over the Arctic. The characteristics of the corresponding surface winds derived from the regression are well aligned to the isolines of the pressure anomalies and thus in line with the geostrophic balance assumed before.

We now attempt to find a functional relation between the CESM surface winds—as represented by the PCs of the four leading EOF patterns of the SLP (Figure 3)—and OBP taken from the same model run. By employing a robust multiple linear regression approach [*Holland and Welsch* 1977], we find that the PCs one (regression coefficient $s = 1.2187$), two ($s = -0.7607$), and four ($s = 0.7147$) are important for reconstructing the time series of the North Pacific mass variation simulated in CESM from atmospheric quantities, whereas the third pattern ($s = -0.0101$) can be safely neglected. Note that neither employing a simple linear regression approach, nor including additional indices as predictors—we tested for example indices for the Solar Cycle and for the Quasi Biennial Oscillation—significantly alters the results.

The PCs one, two, and four as well as their corresponding regression coefficients are subsequently applied to reconstruct OBP from CESM SLP fields (Figure 4). The reconstruction compares well to the time series of OBP simulated in the model: in particular, it captures all major features with realistic amplitudes. Both time series correlate with 0.89 over the whole 145 years of the CESM experiment. The histogram of the residuals (Figure 5a) is approximately normally distributed, suggesting that no major systematic effects have been omitted in the functional model applied for the reconstruction.

5. Reconstruction of OBP From ERA-Interim SLP

Since OBP in the North Pacific is well reconstructed from only three modes of the atmospheric sea-level pressure in CESM, it is straightforward to test whether the functional relationship identified in the CESM

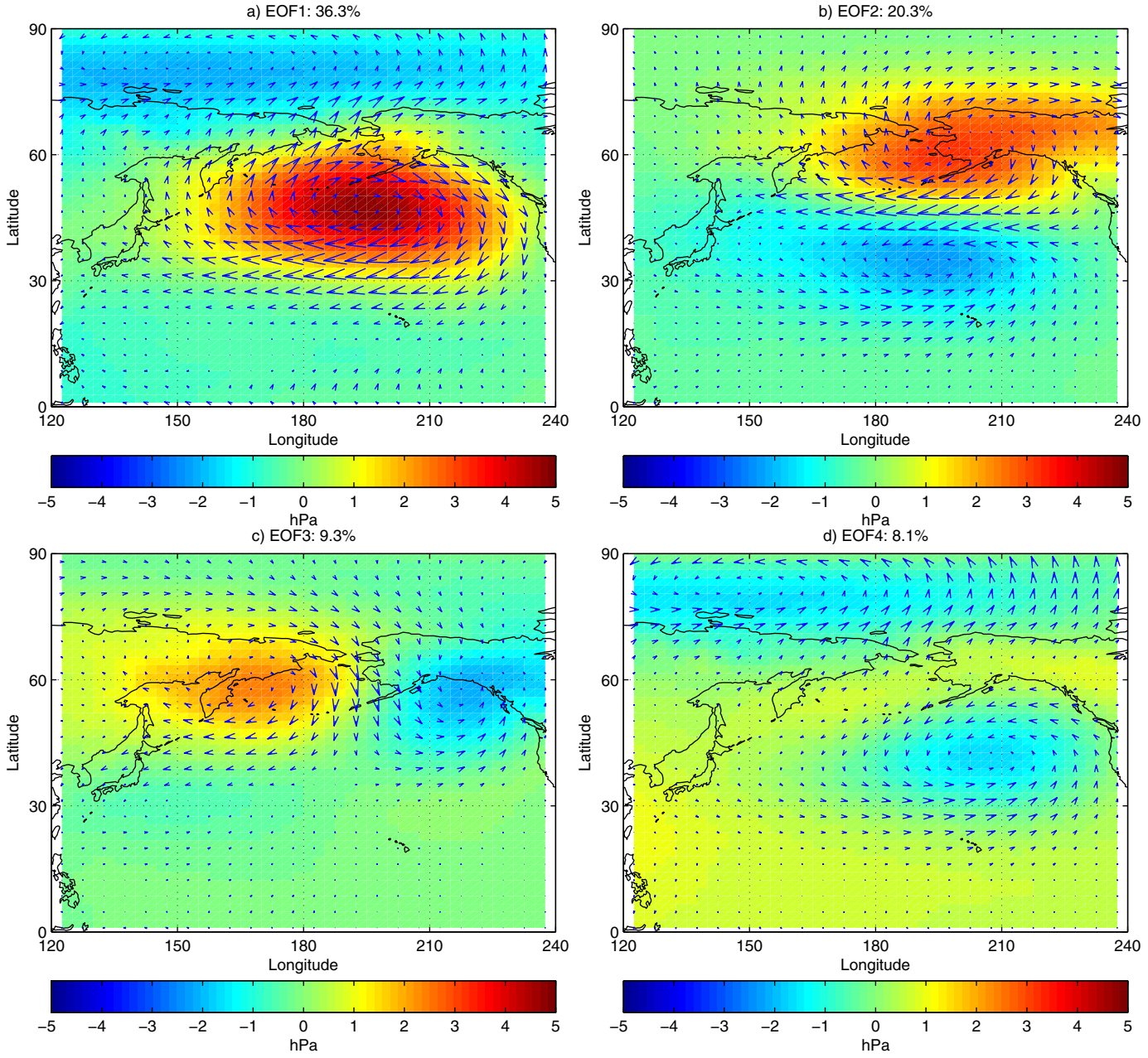

Figure 2. Leading four EOFs computed of detrended and deseasonalized atmospheric sea-level pressure from the 145 year-long CESM experiment. The vector field overlaid to the atmospheric pressure patterns indicates the corresponding surface wind field.

climate model experiment is transferable (i) to realistic wind and pressure distributions as synthesized by a modern atmospheric reanalysis like ERA-Interim, and (ii) to measured OBP variations as observed by the satellite mission GRACE. From ERA-Interim, SLP fields and surface wind fields are available for this study over 24 years since 1989. For this period, also simulated OBP from an OMCT experiment forced with ERA-Interim is available. GRACE OBP observations were acquired only in the second half of this period, between 2003 and 2012.

We project ERA-Interim SLP grids onto the three relevant EOF modes obtained from CESM and thereby obtain three quasi PCs. Those quasi PCs are introduced into the regression model derived in the previous section in order to again reconstruct the OBP variability from atmospheric conditions alone (Figure 6). Compared to the simulated mass anomalies from OMCT, we note a generally good correspondence of the

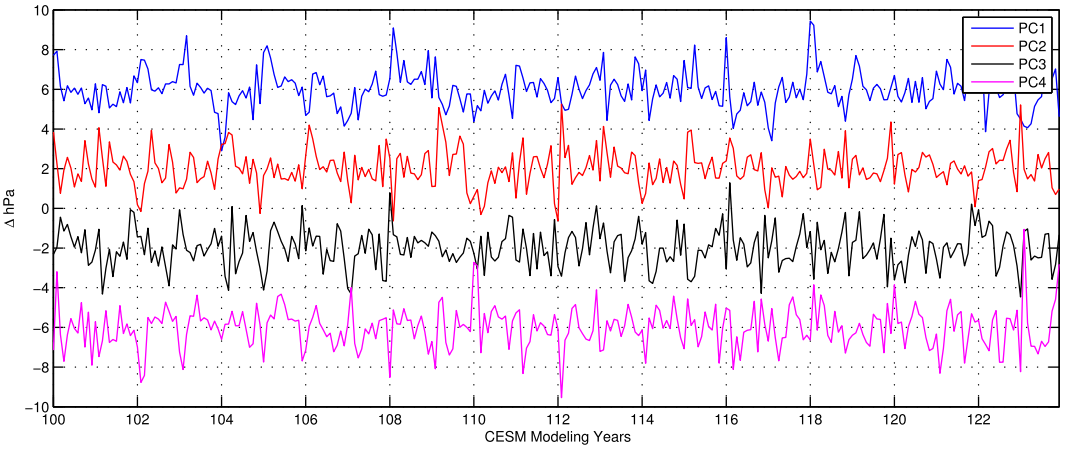

Figure 3. Time series covering the simulated years 100–124 of the principal components associated with the four leading EOF modes computed from the 145 year-long CESM experiment. Individual PCs have been shifted vertically to allow for better readability.

regression results as indicated by a correlation of 0.85. Amplitudes of the reconstruction are somewhat weaker than the OMCT results, but anomalous peaks are generally well captured by the reconstruction.

Over the GRACE mission period, the correlation of the reconstruction with the satellite OBP observations is lower (r=0.70), whereas correlation with OMCT OBP remains at 0.85 also for this single decade. However, amplitudes of the reconstructed signals are closer to the GRACE estimates than those of OMCT, a result that is in line with previous findings of generally too high variability in the 1.875° configuration of OMCT. In a more recent configuration of this numerical ocean model, these signal amplitudes are smaller and more in line with GRACE observations [*Dobslaw et al*. 2013]. Deviations from the normal distribution in the histograms of the residuals (Figure 5) are not significant due to the limited number of samples available for the GRACE period. We therefore see clear empirical evidence that observed OBP variability in the North Pacific is explained to a large extent by changes in the surface winds in the larger North Pacific area.

6. Relation of OBP to Dedicated Climate Modes

We now assess the question whether OBP variability in the central North Pacific as observed by GRACE is related to a single mode of climate variability in the coupled atmosphere-ocean system. We are in particular interested in this question, since a number of previous studies that analyzed GRACE-based OBP in the same area arrived at the conclusion that OBP observed by GRACE is related to the El Niño Southern Oscillation (ENSO) on interannual timescales [*Song and Zlotnicki* 2008; *Chambers* 2011]. If that would be indeed the

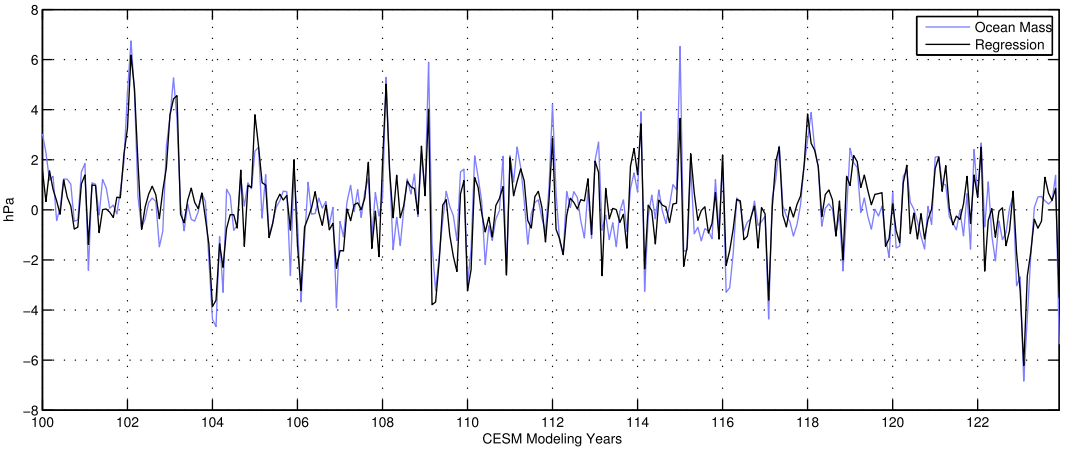

Figure 4. Time variations of ocean bottom pressure averaged over the North Pacific as indicated in Figure 1 from the CESM experiment (blue line), and as reconstructed from atmospheric sea-level pressure and the regression coefficients given in Figure 3 (black line). The correlation between the simulated ocean bottom pressure and the reconstruction over the whole 145 years long period is r = 0.89.

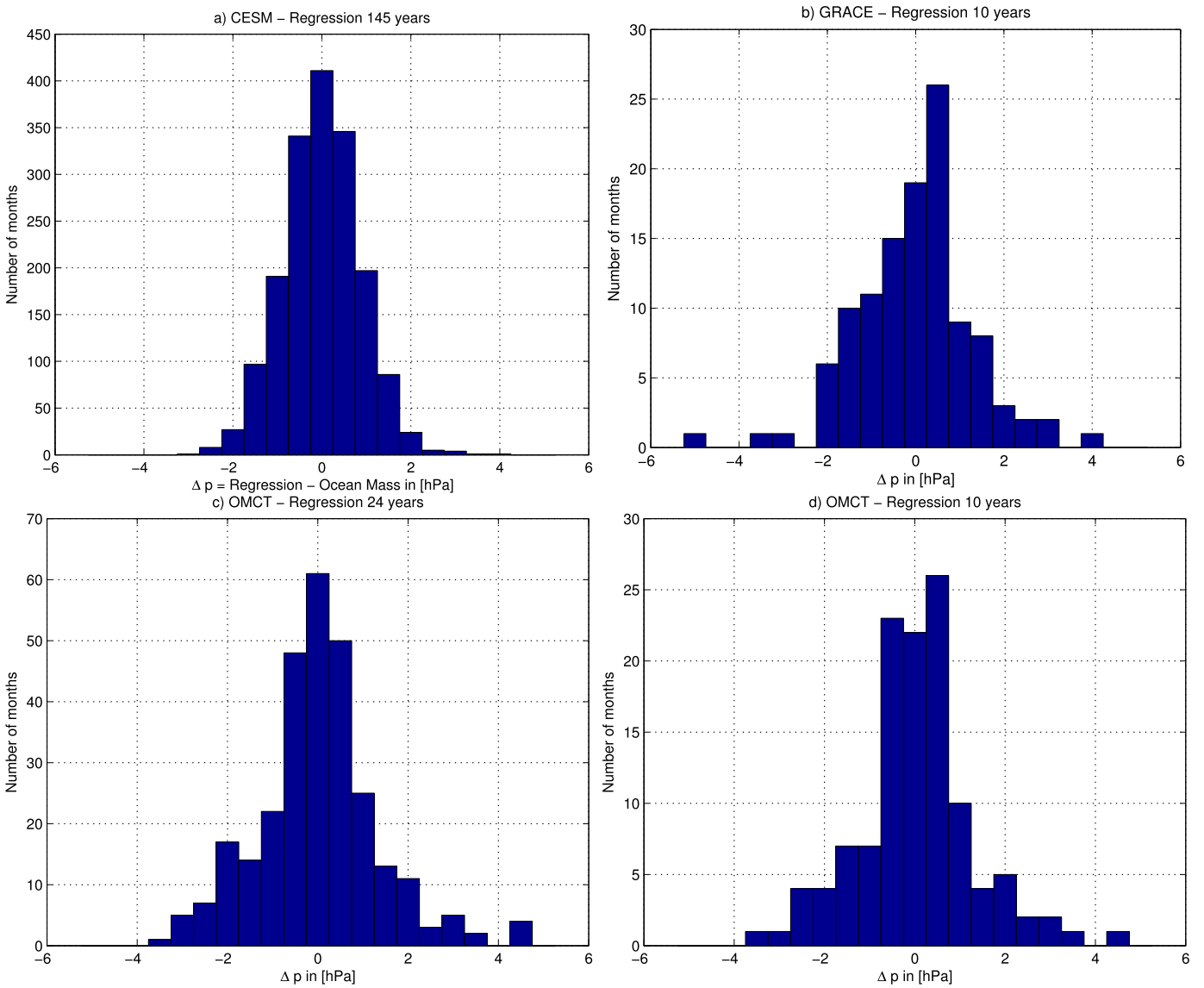

Figure 5. Histograms of the residuals between the reconstructed and simulated or observed ocean bottom pressure for (a) the 145 years long CESM experiment, (b) 10 years of GRACE observations, (c) from 24 years of OMCT simulations forced with ERA-Interim, and (d) from 10 years of OMCT simulations forced with ERA-Interim that are concurrent with the available GRACE observations.

case, GRACE OBP might be in principle considered as an additional proxy to represent that particular mode within a composite index as the Multivariate El Nino Southern Oscillation Index [*Wolter and Timlin* 1998].

As the most prominent mode of interhemispheric large-scale climate variability, ENSO is driven by atmosphere-ocean interactions in the tropics [*Neelin et al.* 1998; *Chang et al.* 2006], and is known to have a number of teleconnections to middle and high latitudes. Here, we represent ENSO by means of the Southern Oscillation Index (SOI), which is defined as the double-standardized difference in sea-level pressure between Tahiti (131° E; 13° S) and Darwin (210° E; 18° S).

As an alternative explanation, however, we consider the Northern Annular Mode (NAM), which describes most of the nonseasonal atmospheric variability in the northern extratropics [*Thompson and Wallace* 2000]. The NAM explains about 20–30% of the total variance of the deseasonalized wind and geopotential height fields and represents a meridional north-south shift of atmospheric masses, which coincides with a north-south vacillation of the wind field around 55°–60° N and 30°–35° N. A typical definition of the NAM index as given by *Baldwin and Thompson* [2009] considers the principal component of the first empirical

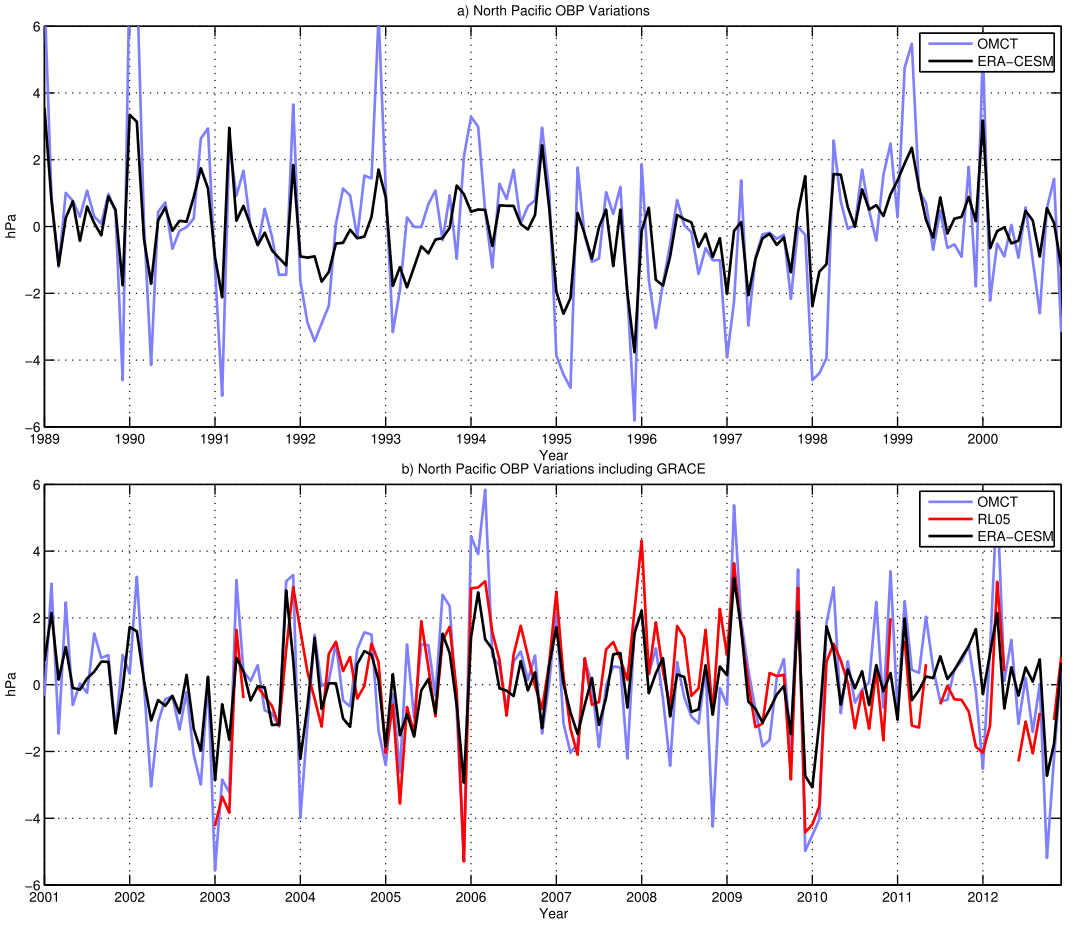

Figure 6. Time variations of ocean bottom pressure averaged over the North Pacific as indicated in Figure 1 from the OMCT experiment forced with ERA-Interim (blue line), as observed by the satellite gravity mission GRACE (red line) and as reconstructed from atmospheric sea-level pressure from ERA-Interim (black line). The correlation between the ocean bottom pressure from GRACE and the reconstruction over the 10 years long observational period is r = 0.7.

orthogonal function of the deseasonalized sea-level pressure north of 20° N. With those definitions, we calculate SOI and NAM indices for both ERA-Interim and the CESM experiment.

To analyze the relations between the different climate modes and OBP, we calculate composite mean differences between maximum and minimum conditions of the related index. For this, maximum conditions are defined by an index exceeding one standard deviation, while minimum months need to have an index of < -1 standard deviation. For ENSO (Figure 7), we note that the average Aleutian Low centered at 45° N, 160° W is about 7 hPa lower during El Niño compared to La Niña in both CESM and ERA-Interim. This is generally in line with the findings of *Niebauer* [1988] who describes the Aleutian Low to be about 2 hPa below average during El Niño and about 3 hPa above average during La Niña, as long as only winter months are considered. More recent assessments [e.g., *Trenberth et al*. 1998] generally confirm this relationship. In terms of OBP, we find for El Niño a negative pressure anomaly at the northern flank of the subtropical gyre. Both CESM and GRACE show in general a consistent pattern here, the shift of the OBP anomaly toward the north-east is more likely related to sampling issues in the rather short observational period of GRACE.

Furthermore, the composite mean differences for the NAM (Figure 8) show a quite similar picture. For the SLP, we identify a dominating pressure anomaly in the eastern part of the North Pacific that is even more enhanced (10 hPa) than the anomalous Aleutian Low identified during El Niño conditions. Those changes in atmospheric surface pressure and in the accompanying wind fields lead to notable changes in OBP in the western North Pacific of more than 2 hPa in the observations, and even slightly larger anomalies in the CESM climate model experiment.

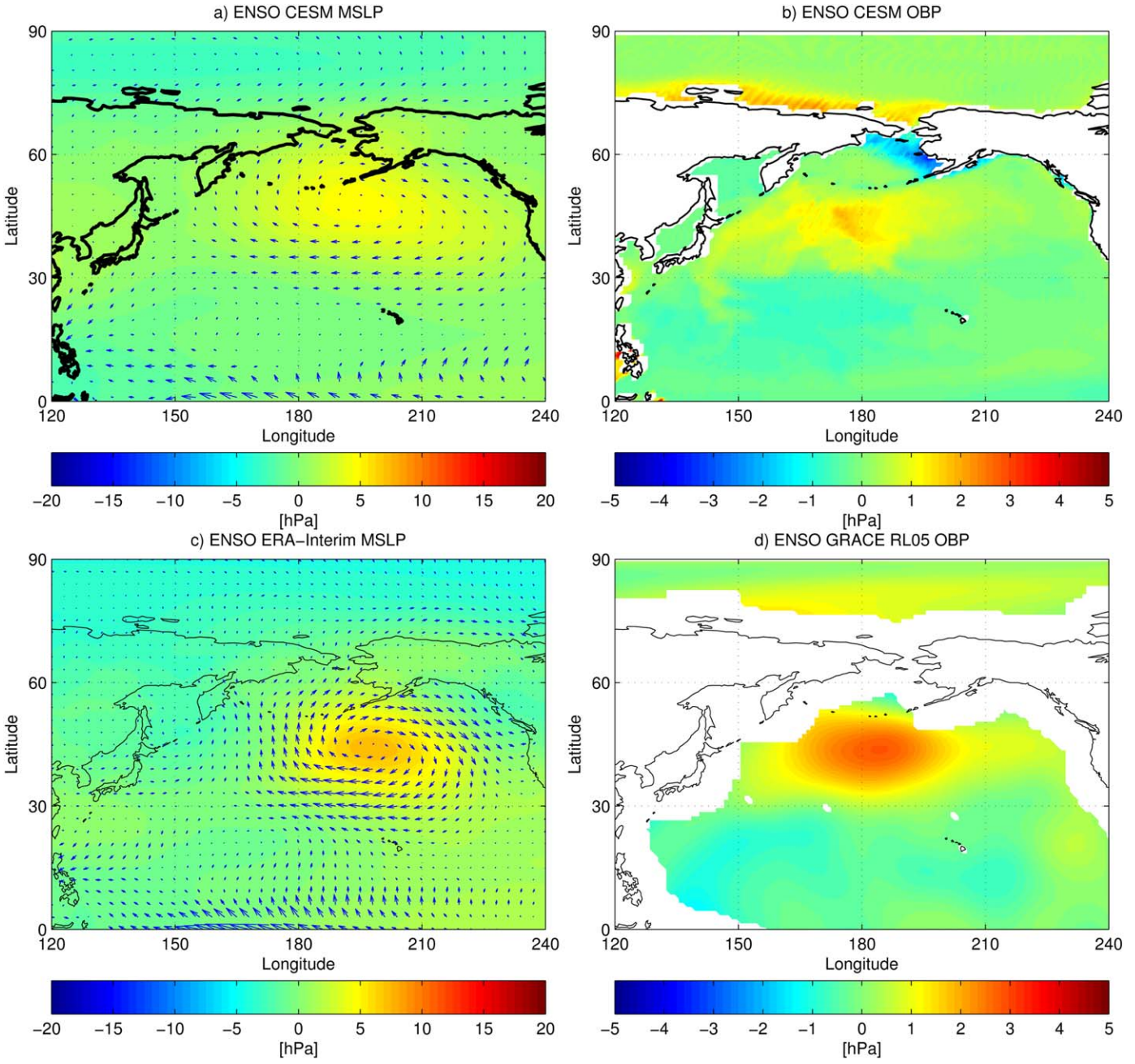

Figure 7. Composite mean differences for the Southern Oscillation Index (Min-Max) of atmospheric sea-level pressure (left) and ocean bottom pressure from the 145 year-long CESM experiment (top) and 10 years of ERA-Interim atmospheric pressure and GRACE ocean bottom pressure (bottom). The associated surface wind anomalies are overlaid to the atmospheric pressure anomalies by means of vector plots.

Those results on the impact of both tropical and extratropical climate modes on the North Pacific OBP variability are well in line with an analysis of the driving processes of the North Pacific atmospheric jets based on ERA-40 re-analysis data [*Li and Wettstein* 2012]. For an extended winter season (November to April), those authors find that the subtropical jet over the North Pacific is both thermally and eddy-driven, thereby rather corresponding to the idealized "combined jet" model of *Lee and Kim* [2003]. Since thermal driving essentially originates in the tropics and is communicated to higher latitudes by means of a time-variable Hadley circulation, whereas eddy momentum flux convergence is rather related to midlatitude dynamics, it is plausible that near surface wind conditions and thus OBP variability in the North Pacific are both correlated to indices that characterize tropical and extratropical atmospheric variability.

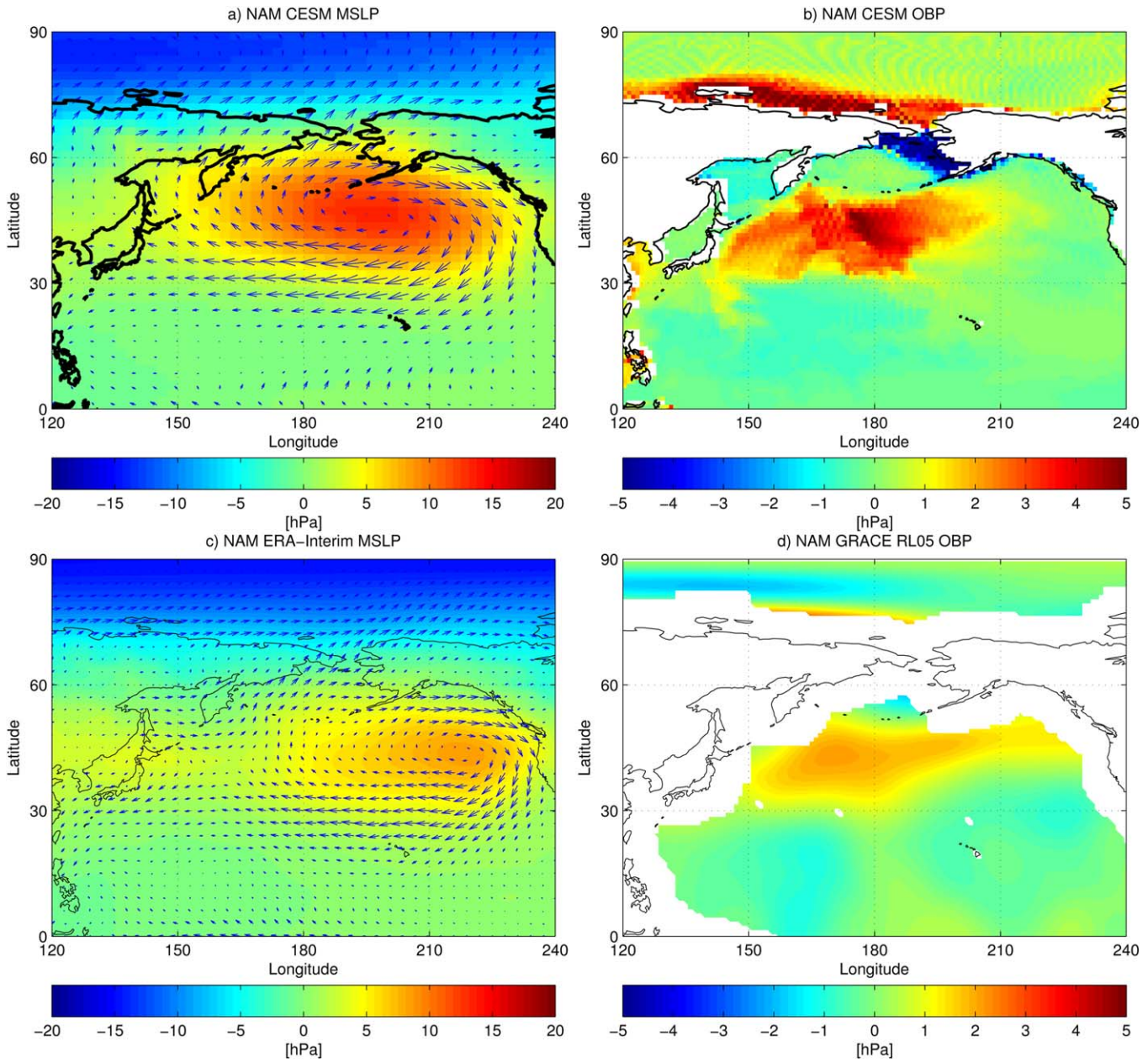

Figure 8. Composite mean differences for the NAM index (Min-Max) of atmospheric sea-level pressure (left) and ocean bottom pressure from the 145 year-long CESM experiment (top) and 10 years of ERA-Interim atmospheric pressure and GRACE ocean bottom pressure (bottom). The associated surface wind anomalies are overlaid to the atmospheric pressure anomalies by means of vector plots.

Beyond ENSO and NAM, there are several other natural climate variability modes that characterize the atmospheric circulation pattern in the North Pacific. For example, the Pacific Decadal Oscillation [*Mantua and Hare* 2002], typically characterized by a distinct temperature anomaly in the subtropical North Pacific, is also connected with a sea level anomaly of about 2 hPa centered at the Aleutian Islands. Since this region largely overlaps areas of SLP pressure changes related to ENSO and the NAM, and since it moreover has been identified previously as a place where wind changes affect the OBP variability in the western subtropical North Pacific, we conclude that it is not possible to relate observed OBP anomalies unambiguously to only one single climate mode, be it ENSO, NAM, or the PDO. It is rather the surface wind regime of a wide area in the North Pacific that is reflected in the OBP.

7. Summary

With the GRACE mission in orbit since 2002 and GRACE Follow-On in preparation for launch in 2017, it is now feasible to monitor mass transport processes in the Earth system with monthly resolution at regional scales larger than a few hundred kilometers in diameter. The mission concept essentially senses mass anomalies on and below the Earth's surface, thereby allowing to measure large-scale OBP variability and their spatial gradients over the global oceans from space.

While disregarding eustatic sea-level variations related to mass exchange between continents and oceans, OBP variability on regional scales is approximately explained by a local Sverdrup balance, relating the time-variable mass transport to changes of the vertical component of the wind stress curl. At periods away from the seasonal cycle, such signals are particularly prominent at moderate latitudes as, for example, in the western subtropical North Pacific. By means of a multiple linear regression analysis of a 145 year-long climate model integration, we have shown that simulated OBP variability is reasonably well-reconstructed from only three dominant variability modes of the atmospheric sea-level pressure in the North Pacific region. Since OBP variability from GRACE is equally well-explained by the atmospheric pressure from ERA-Interim, we conclude that GRACE-based OBP observations indeed carry integrated information about the atmospheric surface pressure and wind field in the North Pacific area.

Although alternative ways exist for observing the large-scale pressure and wind variability over the extratropical North Pacific, we argue that GRACE-based OBP can be considered as a potential source of information for the atmospheric conditions in the region. To explore this in detail, however, tailored data assimilation studies following, e.g., the experimental set-up of *Neef and Matthes* [2012] need to be performed. Best results are expected during boreal winter, where barotropic conditions dominate and surface wind characteristics are therefore representative for the large-scale atmospheric flow in the lower troposphere.

We do not find, however, North Pacific OBP as observed by GRACE to be related solely to ENSO as it has been suggested in previous studies [*Song and Zlotnicki* 2008; *Chambers* 2011]. Instead, we find also evidence of an influence of extratropical atmospheric variability as characterized by the NAM on the surface winds. This is consistent with an assessment of the characteristics of the subtropical atmospheric jet over the North Pacific region by *Li and Wettstein* [2012], who found this jet to be driven both by tropical convection as well as by extratropical eddy momentum flux convergence. We therefore conclude that—instead of being representative of any single climate index—GRACE-based OBP is an integrated measure of the atmospheric surface pressure and wind conditions in the larger North Pacific area.

Acknowledgments

GRACE observations and OMCT model data are publicly available at isdc.gfz-potsdam.de/grace. We thank Deutscher Wetterdienst, Offenbach, Germany, and the European Centre for Medium-Range Weather Forecasts, Reading, U.K., for providing data from ECMWF's latest reanalysis ERA-Interim. CESM and OMCT simulations were performed at Deutsches Klimarechenzentrum, Hamburg, Germany. This study has been carried out within the Helmholtz-University Young Investigators Group NATHAN, funded by the Helmholtz-Association through the President's Initiative and Networking Fund, Deutsches GeoForschungsZentrum (GFZ), GEOMAR Helmholtz Centre for Ocean Research Kiel, and Free University Berlin. Additional support has been provided by the German Federal Ministry of Education and Research (BMBF) within the FONA research program under grants 03F0654A and 01LP1151A.

References

Baldwin, M., and D. Thompson (2009), A critical comparison of stratosphere-troposphere coupling indices, *Q. J. Roy. Met. Soc.*, *135*, 1661–1672, doi:10.1002/qj.

Barnston, A., and R. Livezey (1987), Classification, seasonality and persistence of low-frequency atmospheric circulation patterns, *Mon. Weather Rev.*, *115*(6), 1083–1126.

Bergmann, I., and H. Dobslaw (2012), Short-term transport variability of the Antarctic Circumpolar Current from satellite gravity observations, *J. Geophys. Res.*, *117*, C05044, doi:10.1029/2012JC007872.

Bingham, R. J., and C. W. Hughes (2006), Observing seasonal bottom pressure variability in the North Pacific with GRACE, *Geophys. Res. Lett.*, *33*, L08607, doi:10.1029/2005GL025489.

Chambers, D. P. (2011), ENSO-correlated fluctuations in ocean bottom pressure and wind-stress curl in the North Pacific, *Ocean Sci.*, *7*(5), 685–692, doi:10.5194/os-7-685-2011.

Chambers, D. P., and J. A. Bonin (2012), Evaluation of Release-05 GRACE time-variable gravity coefficients over the ocean, *Ocean Sci.*, *8*(5), 859–868, doi:10.5194/os-8-859-2012.

Chambers, D. P., and J. K. Willis (2010), A Global Evaluation of Ocean Bottom Pressure from GRACE, OMCT, and Steric-Corrected Altimetry, *J. Atmos. Oceanic Technol.*, *27*(8), 1395–1402, doi:10.1175/2010JTECHO738.1.

Chang, P., T. Yamagata, and P. Schopf (2006), Climate fluctuations of tropical coupled systems-the role of ocean dynamics, *J. Clim.*, *19*, 5122–5174.

Cheng, X., L. Li, Y. Du, J. Wang, and R.-X. Huang (2013), Mass-induced sea level change in the northwestern North Pacific and its contribution to total sea level change, *Geophys. Res. Lett.*, *40*, 3975–3980, doi:10.1002/grl.50748.

Dahle, C., F. Flechtner, C. Gruber, D. Koenig, R. Koenig, G. Michalak, and K.-H. Neumeyer (2012), GFZ GRACE Level-2 Processing Standards Document for Level-2 Product Release 0005, *Scientific Technical Report STR 12/02*, *20*, doi:10.2312/GFZ.b103-12020.

Danabasoglu, G., S. C. Bates, B. P. Briegleb, S. R. Jayne, M. Jochum, W. G. Large, S. Peacock, and S. G. Yeager (2012), The CCSM4 Ocean Component, *J. Clim.*, *25*(5), 1361–1389, doi:10.1175/JCLI-D-11-00091.1.

Dee, D. P., et al. (2011), The ERA-Interim reanalysis: Configuration and performance of the data assimilation system, *Q. J. R. Meterol. Soc.*, *137*(656), 553–597, doi:10.1002/qj.828.

Dobslaw, H. (2007), Modellierung der allgemeinen ozeanischen Dynamik zur Korrektur und Interpretation von Satellitendaten, *Sci. Tech. Rep. 07/10*, Deutsches GeoForschungsZentrum, Potsdam, doi:10.2312/GFZ.b103-07103.

Dobslaw, H., and M. Thomas (2007a), Simulation and observation of global ocean mass anomalies, *J. Geophys. Res.*, *112*, C05040, doi: 10.1029/2006JC004035.
Dobslaw, H., and M. Thomas (2007b), Impact of river run-off on global ocean mass redistribution, *Geophys. J. Int.*, *168*(2), 527–532, doi: 10.1111/j.1365-246X.2006.03247.x.
Dobslaw, H., F. Flechtner, I. Bergmann-Wolf, C. Dahle, R. Dill, S. Esselborn, I. Sasgen, and M. Thomas (2013), Simulating high-frequency atmosphere-ocean mass variability for dealiasing of satellite gravity observations: AOD1B RL05, *J. Geophys. Res.*, *118*, 3704–3711, doi: 10.1002/jgrc.20271.
Drijfhout, S., C. Heinze, M. Latif, and E. Maier-Reimer (1996), Mean circulation and internal variability in an ocean primitive equation model, *J. Phys. Oceanogr.*, *26*, 559–580.
Eanes, R. (2000), SLR solutions from the University of Texas Center for Space Research, Geocenter from TOPEX SLR/DORIS, 1992–2000, technical report, IERS Spec. Bur. for Gravity/Geocenter, Pasadena, Calif.
Flechtner, F., H. Dobslaw, and E. Fagiolini (2013), GRACE AOD1B Product Description Document for AOD1B Product Description Document for Product Release 05, Tech. Rep., Rev. 4.0, GRACE Document 327–750, GeoForschungsZentrum Potsdam.
Gent, P. R., et al. (2011), The community climate system model version 4, *J. Clim.*, *24*(19), 4973–4991, doi:10.1175/2011JCLI4083.1.
Gill, A. E., and P. P. Niiler (1973), The theory of the seasonal variability in the ocean, *Deep Sea Res. Oceanogr. Abstr.*, *20*(9), 141–177.
Holland, P., and R. Welsch (1977), Robust regression using iteratively reweighted least-squares, *Commun. Stat. Theory*, *6*(9), 37–41.
Hollmann, R., C. J. Merchant, R. Saunders, C. Downy, M. Zaitchik, and W. Cazenave, and W. Wagner (2013), The ESA Climate Change Initiative: Satellite data records for essential climate variables, *Bull. A. Met. Soc.*, *94*, 1541–1552, doi:10.1175/BAMS-D-11-00254.1.
Houborg, R., M. Rodell, B. Li, R. Reichle, and B. F. Zaitchik (2012), Drought indicators based on model-assimilated Gravity Recovery and Climate Experiment (GRACE) terrestrial water storage observations, *Water Ressour. Res.*, *48*, W07525, doi:10.1029/2011WR011291.
Hughes, C. W., M. E. Tamisiea, R. J. Bingham, and J. Williams (2012), Weighing the ocean: Using a single mooring to measure changes in the mass of the ocean, *Geophys. Res. Lett.*, *39*, L17602, doi:10.1029/2012GL052935.
Jacob, T., J. Wahr, W. T. Pfeffer, and S. Swenson (2012), Recent contributions of glaciers and ice caps to sea level rise., *Nature*, *482*, 514–518, doi:10.1038/nature10847.
Kusche, J. (2007), Approximate decorrelation and non-isotropic smoothing of time-variable GRACE-type gravity field models, *J. Geod.*, *81*(11), 733–749, doi:10.1007/s00190-007-0143-3.
Lawrence, D. M., et al. (2011), Parameterization improvements and functional and structural advances in Version 4 of the Community Land Model, *J. Adv. Model. Earth Syst.*, *3*, M03001, doi:10.1029/2011MS000045.
Lee, S., and H. Kim (2003), The dynamical relationship between subtropical and eddy-driven jets, *J. Atmos. Sci.*, *60*, 1490–1503.
Li, C., and J. J. Wettstein (2012), Thermally driven and eddy-driven jet variability in reanalysis, *J. Clim.*, *25*(5), 1587–1596, doi:10.1175/JCLI-D-11-00145.1.
Liu, Z., and M. Alexander (2007), Atmospheric bridge, oceanic tunnel, and global climatic teleconnections, *Rev. Geophys.*, *45*, RG2005, doi: 10.1029/2005RG000172.1.INTRODUCTION.
Lorbacher, K., S. J. Marsland, J. A. Church, S. M. Griffies, and D. Stammer (2012), Rapid barotropic sea level rise from ice sheet melting, *J. Geophys. Res.*, *117*, C06003, doi:10.1029/2011JC007733.
Mantua, N., and S. Hare (2002), Pacific decadal oscillation, *J. Oceanogr.*, *1*, 592–594.
Marsh, D. R., M. J. Mills, D. E. Kinnison, J.-F. Lamarque, N. Calvo, and L. M. Polvani (2013), Climate Change from 1850 to 2005 Simulated in CESM1(WACCM), *J. Clim.*, *26*(19), 7372–7391, doi:10.1175/JCLI-D-12–00558.1.
Moon, J.-H., and Y. T. Song (2013), Sea level and heat content changes in the western North Pacific, *J. Geophys. Res. Oceans*, *118*, 2014–2022, doi:10.1002/jgrc.20096.
Neale, R. B., J. Richter, S. Park, P. H. Lauritzen, S. J. Vavrus, P. J. Rasch, and M. Zhang (2013), The mean climate of the community atmosphere model (CAM4) in forced SST and fully coupled experiments, *J. Clim.*, *26*(14), 5150–5168, doi:10.1175/JCLI-D-12-00236.1.
Neef, L. J., and K. Matthes (2012), Comparison of Earth rotation excitation in data-constrained and unconstrained atmosphere models, *J. Geophys. Res.*, *117*, D02107, doi:10.1029/2011JD016555.
Neelin, J., D. S. Battisti, A. Hirst, F. Jin, Y. Wakata, T. Yamagata, and S. E. Zebiak (1998), ENSO theory, *J. Geophys. Res.*, *103*(C7), 14,261–14,290, doi:10.1029/97JC03424.
Niebauer, H. (1988), Effects of El Nino-Southern oscillation and north pacific weather patterns on interannual variability in the Subarctic Bering sea, *J. Geophys. Res.*, *93*(5), 5051–5068, doi:10.1029/JC093iC05p05051.
Petrick, C. (2013), Validating modeled climate variations using geodetic monitoring data, PhD thesis, Free Univ. Berlin, Germany.
Ponte, R. M. (1999), A preliminary model study of the large-scale seasonal cycle in bottom pressure over the global ocean, *J. Geophys. Res.*, *104*(C1), 1289–1300, doi:10.1029/1998JC900028.
Sakumura, C., S. Bettadpur, and S. Bruinsma (2014), Ensemble prediction and intercomparison analysis of GRACE time-variable gravity field models, *Geophys. Res. Lett.*, *41*, 1389–1397, doi:10.1002/2013GL058632.1.
Song, Y. T., and V. Zlotnicki (2008), Subpolar ocean bottom pressure oscillation and its links to the tropical ENSO, *Int. J. Remote Sens.*, *29*(21), 6091–6107, doi:10.1080/01431160802175538.
Tamisiea, M. E., E. M. Hill, R. M. Ponte, J. L. Davis, I. Velicogna, and N. T. Vinogradova (2010), Impact of self-attraction and loading on the annual cycle in sea level, *J. Geophys. Res.*, *115*, C07004, doi:10.1029/2009JC005687.
Tapley, B. D., S. Bettadpur, J. C. Ries, P. F. Thompson, and M. M. Watkins (2004), GRACE measurements of mass variability in the Earth system, *Science*, *305*(5683), 503–505, doi:10.1126/science.1099192.
Thomas, M., J. Sündermann, and E. Maier-Reimer (2001), Consideration of ocean tides in an OGCM and impacts on subseasonal to decadal polar motion, *Geophys. Res. Lett.*, *28*(12), 2457–2460, doi:10.1029/2000GL012234.
Thompson, D. W. J., and J. M. Wallace (2000), Annular modes in the extratropical circulation. Part I: Month-to-month variability, *J. Clim.*, *13*(5), 1000–1016, doi:10.1175/1520-0442(2000)013¡1000:AMITEC¿2.0.CO;2.
Trenberth, K. E., G. W. Branstator, D. Karoly, A. Kumar, N.-C. Lau, and C. Ropelewski (1998), Progress during TOGA in understanding and modeling global teleconnections associated with tropical sea surface temperatures, *J. Geophys. Res.*, *103*(C7), 14,291–14,324, doi:10.1029/97JC01444.
Voss, K. a., J. S. Famiglietti, M. Lo, C. Linage, M. Rodell, and S. C. Swenson (2013), Groundwater depletion in the Middle East from GRACE with implications for transboundary water management in the Tigris-Euphrates-Western Iran region, *Water Ressour. Res.*, *49*, 904–914, doi:10.1002/wrcr.20078.
Wahr, J., M. Molenaar, and F. Bryan (1998), Time variability of the Earth's gravity field: Hydrological and oceanic effects and their possible detection using GRACE, *J. Geophys. Res.*, *103*(B12), 30,205–30,229, doi:10.1029/98JB02844.
Wolff, J. J.-O., E. Maier-Reimer, and S. Legutke (1997), *The Hamburg Ocean Primitive Equation Model*, vol. 13, pp. 1–110, DKRZ, Hamburg, Germany.
Wolter, K., and M. Timlin (1998), Measuring the strength of ENSO events: How does 1997/98 rank?, *Weather*, *53*(9), 315–324.